

CdZnTe Background Measurement at Balloon Altitudes with an Active BGO Shield

P. Bloser^a, J. Grindlay^a, T. Narita^a, and F. Harrison^b

^aHarvard-Smithsonian Center for Astrophysics, 60 Garden St., Cambridge, MA 02138, USA

^bSpace Radiation Laboratory, 220-47 California Institute of Technology, Pasadena, CA 91125, USA

ABSTRACT

We report results of an experiment conducted in May 1997 to measure CdZnTe background and background reduction schemes in space flight conditions similar to those of proposed hard X-ray astrophysics missions. A 1 cm² CdZnTe detector was placed adjacent to a thick BGO anticoincidence shield and flown piggybacked onto the EXITE2 scientific balloon payload. The planar shield was designed to veto background counts produced by local gamma-ray production in passive material and neutron interactions in the detector. The CdZnTe and BGO were partially surrounded by a Pb-Sn-Cu shield to approximate the grammage of an X-ray collimator, although the field of view was still $\sim 2\pi$ sr. At an altitude of 127000 feet we find a reduction in background by a factor of 6 at 100 keV. The non-vetoed background is 9×10^{-4} cts cm⁻² s⁻¹ keV⁻¹ at 100 keV, about a factor of 2 higher than that of the collimated (4.5° FWHM) EXITE2 phoswich detector. We compare our recorded spectrum with that expected from simulations using GEANT and find agreement within a factor of 2 between 30 and 300 keV. We also compare our results with those of previous experiments using passive lead and active NaI shields, and discuss possible active shielding schemes in future astronomy missions employing large arrays of CdZnTe detectors.

Keywords: CdZnTe, background, shielding, balloon flights, hard X-ray astronomy, instrumentation

1. INTRODUCTION

The somewhat primitive state of hard X-ray and soft gamma-ray detector technology has been given a boost in recent years by the emergence of Cadmium Zinc Telluride (CdZnTe) as an effective wide-bandgap, high-density semiconductor detector.¹ Historically, creating imaging instruments in the hard X-ray range (~ 20 –500 keV) has been especially difficult, since energies are too high for multi-layer focusing optics ($\lesssim 80$ keV) and too low for Compton telescopes ($\gtrsim 500$ keV). The only practical method for imaging in this band is the coded aperture technique, in which the position of the X-ray source can be deduced from the shadow cast by a specially-designed mask onto a large-area, position-sensitive detector. Although successfully employed in many experiments, telescopes based on this principle have suffered from the poor spatial and energy resolution of the scintillator detectors (NaI, CsI, etc.) used to date. CdZnTe is an attractive alternative since it has the good energy resolution of a semiconductor, yet has far higher stopping power than silicon and does not require cryogenic cooling like germanium. Of concern is the poor mobility-lifetime ($\mu\tau$) product for holes, which can result in poor charge collection and degraded energy resolution. Fortunately, it has been found that employing a grid of pixels small relative to the detector thickness results in an internal electric field favorable for the collection of the electrons only,² a phenomenon often referred to as the “small pixel effect.” As this is precisely the geometry required for a position-sensitive detector, pixellated arrays of CdZnTe for X-ray astronomy have enjoyed intense scrutiny in recent years.^{3,4,5} Our work in particular has been motivated by the need for a large-area hard X-ray survey telescope, such as the Energetic X-ray Imaging Survey Telescope (EXIST or EXIST-LITE) concept,^{6,7} designed to be sensitive between 20 and 600 keV. Thus we have focused our study on relatively thick (5 mm) CdZnTe detectors fashioned with various types of pixellated arrays, and with these devices we have measured a typical energy resolution of $\sim 4\%$ at 60 keV.^{8,9}

A major concern in any space-based astronomy mission is the level and shape of the detector background. This is especially true of hard X-ray instruments. In coded aperture telescopes the collecting area is no bigger than the detector, and 50% of this area is blocked by the mask. Thick detectors such as those studied for EXIST have an even

Further author information: (Send correspondence to P. Bloser)

P.B.: E-mail: pbloser@cfa.harvard.edu

F.H.: E-mail: fiona@srl.caltech.edu

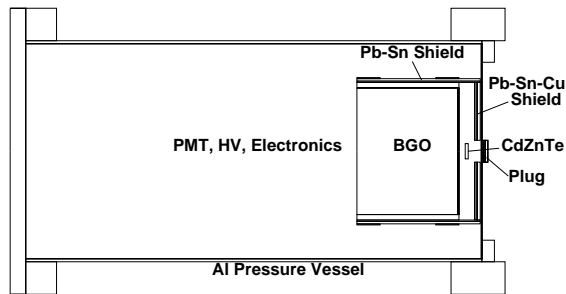


Figure 1. Schematic of the CfA-Caltech CdZnTe/BGO detector. The CdZnTe is 1 cm^2 by 2 mm thick, while the BGO is 8.2 cm diameter \times 6.5 cm thick. The detector is shielded with Pb-Sn-Cu on the front to approximate the grammage of a passive collimator.

more unfavorable ratio of detector volume to collecting area. These considerations are combined with the fact that astrophysical sources are quite weak above $\sim 20 \text{ keV}$, and that the detector is placed in the high-radiation environment of the upper atmosphere or low Earth orbit. The result is that nearly all hard X-ray astronomy observations are completely background dominated, and keeping the background to a minimum is essential for obtaining high signal-to-noise.

The physical processes that produce the primary background components in an instrument are highly dependent on the specific materials used in the detector and the surrounding structures. Typically the background in balloon payloads is due to the combination of diffuse cosmic gamma-rays with gamma-ray photons and energetic particles resulting from cosmic ray interactions in the atmosphere and in the payload itself. Designing effective shielding techniques is thus dependent on a thorough understanding of the interaction processes that dominate when the detector and shields are bombarded with gamma-ray photons, electrons, neutrons, and protons. Much work has been done to measure and characterize the background components in heavily-used detector materials such as NaI and CsI scintillators^{10,11,12} and germanium semiconductors.¹³ A similar effort is required for CdZnTe if its potential as a detector material for astronomy is to be realized. Two measurements of CdZnTe background at balloon altitudes are described in the literature, one each by groups at Goddard Space Flight Center (GSFC)¹⁴ and Caltech,¹⁵ though others exist.¹⁶ These experiments, described in more detail in Sect. 2, employed simple passive and active shielding schemes and represent the first attempts to measure and model the basic physical processes involved. In this work we describe the first experiment designed to measure the in-flight background in a CdZnTe detector in a configuration approximating a real hard X-ray telescope.

2. EXPERIMENTAL CONFIGURATION

As a collaboration between the Harvard-Smithsonian Center for Astrophysics (CfA) and Caltech we have constructed, tested, and flown a single-element CdZnTe detector placed adjacent to a thick BGO anticoincidence shield as a piggyback experiment on the second Energetic X-ray Imaging Telescope Experiment (EXITE2)¹⁷ balloon payload. The design of the instrument was motivated both by the results of previous CdZnTe balloon flights by GSFC¹⁴ and Caltech,¹⁵ and by the requirements of an actual hard X-ray telescope.

The flight of the GSFC CdZnTe experiment PoRTIA, flown in 1995 as a piggyback on the GRIS payload and containing both a thin (2 mm) and thick (5 mm) CdZnTe detector, revealed a background far higher than that of a Ge spectrometer flown alongside.¹⁴ This background was markedly reduced, however, when the CdZnTe detector was surrounded by NaI active shielding. Since a real astronomical instrument cannot completely surround the detector with NaI, the current experiment places the CdZnTe detector directly in front of a thick BGO crystal. The Caltech CdZnTe detector, flown on the GRIP-2 payload, was passively shielded only and showed a high background which has been successfully modeled as gamma-rays produced in the passive material by cosmic ray interactions.¹⁵ Proposed hard X-ray telescopes using CdZnTe, such as EXIST,⁶ usually require some passive material near the detector in the form of a collimator; thus, such material was included in the instrument (although for the balloon-borne EXIST-LITE concept⁷ an active collimator may achieve lower background).

Figure 1 shows a schematic of the CdZnTe/BGO detector, as assembled by Caltech. The detector is housed in an aluminum pressure vessel with an entrance window 20 mil thick. The pressure vessel was filled with nitrogen at ~ 1 atmosphere pressure. The CdZnTe detector was supplied by eV Products and is a planar, single-element device $10\text{ mm} \times 10\text{ mm} \times 2\text{ mm}$. It is centered about 4 mm in front of the BGO, which was supplied by JPL and is 8.2 cm in diameter \times 6.5 cm thick. The BGO thus subtends $\sim 90\%$ of the 2π steradians behind the CdZnTe. The CdZnTe is shielded in the front by 1.8 mm of Pb + 0.85 mm of Sn + 1.2 mm of Cu to approximate the grammage of a graded X-ray collimator. A hole was left in the shield to allow calibration X-ray sources to shine in; this hole was covered by a Pb-Sn-Cu plug attached to the outside of the Al entrance window during flight. The CdZnTe and BGO are shielded on the sides by 1.6 mm of Pb + 0.9 mm of Sn. Within the pressure vessel, behind the BGO, are the readout PMT, high voltage supply biasing the CdZnTe at 300 V, and an eV Products 550 preamp. The detector is connected to an electronics box designed and built at CfA containing shaping amps (shaping time $\sim 3.3\mu\text{s}$) for the CdZnTe and BGO signals, discriminators, and 12-bit ADCs. This box also provided an interface to the main flight computer, which read the CdZnTe/BGO data into the EXITE2 payload’s data stream. The CdZnTe/BGO detector was mounted during flight on the side of the EXITE2 gondola ~ 1.5 m above the primary phoswich detector with the thin Al window pointed straight up.

The CdZnTe/BGO detector was extensively tested and calibrated in the lab at CfA prior to flight using ^{241}Am and ^{133}Ba radioactive sources. We determined the energy range to be $\sim 15\text{--}500$ keV with an energy resolution (FWHM) of 6.2 keV at 60 keV (10.3%). These values were quite stable over periods of time longer than a normal balloon flight ($\gtrsim 24$ hours). The threshold of the BGO shield discriminator was calibrated and set at ~ 30 keV with an uncertainty of 20%. The discriminator is not sharp, but rolls off over ~ 10 keV.

3. FLIGHT RESULTS

The EXITE2 balloon payload, carrying the CdZnTe/BGO detector, was launched from Ft. Sumner, NM at UT 16:15, May 7, 1997. Higher than expected winds forced the flight to be terminated after 14 hours at float altitudes. The altitude varied between 113000 and 127000 feet during the night, corresponding to overlying atmospheric levels between $\sim 6\text{ g cm}^{-2}$ and $\sim 3.5\text{ g cm}^{-2}$. The flight computer system behaved erratically early in the flight, but performed quite well during the second half, and ~ 6000 seconds of good CdZnTe data were collected at the highest altitudes with an average atmospheric grammage of 3.55 g cm^{-2} , as well as ~ 4100 seconds at 5.1 g cm^{-2} and ~ 7300 seconds at 6 g cm^{-2} . After the flight the CdZnTe detector was re-tested in the lab, and the energy calibration was found to be the same as before launch. Thus we believe the detector performance was quite stable during the flight.

Figure 2 shows the EXITE2 CdZnTe spectrum recorded from 6006 seconds of data at an average grammage of 3.55 g cm^{-2} , corresponding to an average altitude of 127423 feet. Both the total events and the “good,” or non-vetoed, events are plotted. The good event rate at 100 keV is $\sim 9 \times 10^{-4}\text{ cts cm}^{-2}\text{ s}^{-1}\text{ keV}^{-1}$, roughly midway between the totally actively-shielded GSFC (PoRTIA) spectrum¹⁴ and the totally passively-shielded Caltech (GRIP-2) spectrum¹⁵ (see Fig. 6). The uncertainty in this background level due to data telemetry throughput uncertainties is less than 5%. The good event rate is a factor of 6 lower than the total event rate at 100 keV, showing that the planar BGO shield placed behind the CdZnTe is an effective means of reducing background. The spectra recorded at 5.1 g cm^{-2} and 6 g cm^{-2} are essentially identical to the spectrum in Fig. 2 at 3.55 g cm^{-2} , ruling out significant effects due to atmospheric depth or time-dependent activation. The EXITE2 CdZnTe flight spectrum will be compared in detail to the PoRTIA and GRIP-2 spectra in Sect. 5.

4. BACKGROUND SIMULATIONS

We have simulated the background recorded by the EXITE2 CdZnTe/BGO detector at 3.55 g cm^{-2} using the CERN Program Library simulation package GEANT. We were able to re-create the geometry of the detector quite accurately, using cylinders, tubes, and boxes of the appropriate materials. (Figure 1, in fact, was produced by GEANT.) Simulations were run recording the energy deposited in both the CdZnTe and the BGO so that both the total and non-vetoed spectra could be reproduced. In this section we detail our simulations and present results.

4.1. Simulating CdZnTe Response

In order to simulate accurately the spectrum recorded in the detector, we had to take into account the response of CdZnTe, specifically charge trapping. Charge is lost from an event when the charge carriers fall into deep traps within the crystal, resulting in low energy tails on recorded spectral lines. The effects of charge trapping on the measured

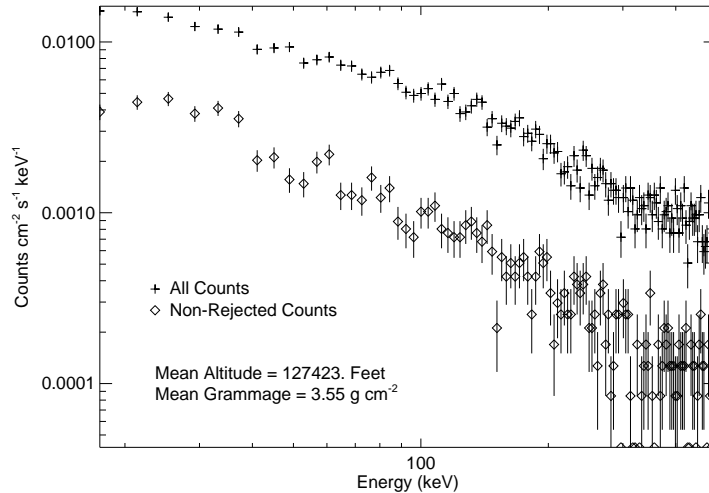


Figure 2. Spectrum recorded by the EXITE2 CdZnTe/BGO detector during flight at an average atmospheric overburden of 3.55 g cm^{-2} . Both total events and non-vetoed events are shown. The non-vetoed event rate is 9×10^{-4} $\text{cts cm}^{-2} \text{ s}^{-1} \text{ keV}^{-1}$ at 100 keV, which is a factor of ~ 6 below the total rate.

pulse height are described by the Hecht equation,¹⁸ which relates the amount of charge collected at the electrodes of a semiconductor device to the depth at which the charge carriers are created, the electric field in the detector, and the mobility-lifetime products for the holes ($\mu_h \tau_h$) and electrons ($\mu_e \tau_e$). Thus we record all the positions at which energy is deposited in the CdZnTe detector during an event, scale each energy according to the Hecht relation, and add up the scaled energies to give the total effective recorded energy for that event. The resulting spectra are then convolved with the detector energy resolution, taken to be a Gaussian with a width of the form $\text{FWHM} = 6.2(E/60)^{1/2} \text{ keV}$.

The electron mobility and lifetime in CdZnTe have been measured quite accurately in the recent literature,¹⁹ and we adopt a typical value of $\mu_e \tau_e = 5 \times 10^{-3} \text{ cm}^2 \text{ V}^{-1}$. The hole parameters are much harder to determine since the holes are so easily trapped. Until recently, values in the literature for $\mu_h \tau_h$ were roughly a factor of 10 less than those for $\mu_e \tau_e$.²⁰ Using $\mu_h \tau_h = 5 \times 10^{-4} \text{ cm}^2 \text{ V}^{-1}$, however, produced simulated spectra that did not show the amount of low energy tailing seen in measured spectra. We determined the best value of $\mu_h \tau_h$ to use by comparing the photopeak efficiencies of the simulated spectra with those of the measured spectra. We fit the X-ray line spectra with a combination of a Gaussian plus an exponential low energy tail, and defined the photopeak efficiency as the ratio of the number of counts under the Gaussian to the total number of counts.^{8,9} Using this method we find reasonable agreement for $\mu_h \tau_h = 3 \times 10^{-5} \text{ cm}^2 \text{ V}^{-1}$. We show typical examples in Fig. 3, comparing recorded ^{241}Am and ^{57}Co spectra to the simulations. For the 60 keV line from ^{241}Am we find photopeak efficiencies of 76% for both the recorded spectrum and the simulated spectrum, while for the 122 keV line from ^{57}Co we find recorded and simulated efficiencies of 29% and 26%, respectively. We note that such low photopeak efficiencies are the result of this detector being a single-element device; a pixellated detector operating in the “small pixel” regime (a 5 mm thick detector with 1.5 mm pixels) gives an efficiency at 60 keV of $\sim 90\%$, as we have reported elsewhere.^{8,9} Such a low value of $\mu_h \tau_h$ has been found elsewhere when comparing simulated charge transport to measurements of CdZnTe.²¹

4.2. Background Components

In this section we describe the various components to the CdZnTe/BGO instrument background that we simulate in our GEANT code. Background is produced by cosmic ray interactions in the atmosphere and payload material, generating both gamma-rays and energetic particles.

4.2.1. Shield Leakage from Atmospheric and Cosmic Diffuse Gamma-Rays

Instruments at balloon altitudes are irradiated by gamma-rays from the diffuse cosmic X-ray and gamma-ray backgrounds and from the atmosphere. The atmospheric gamma-rays are produced mainly by bremsstrahlung from

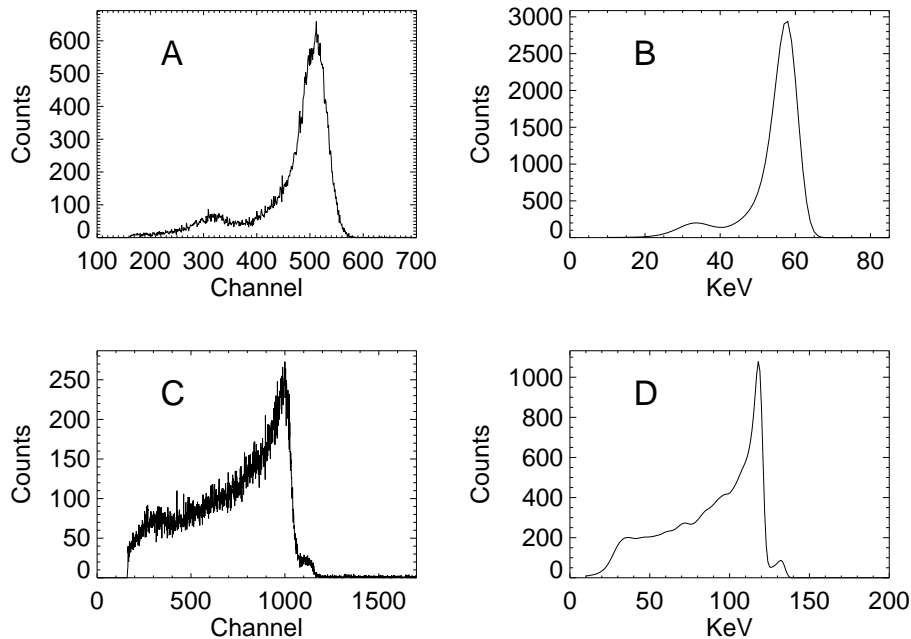


Figure 3. Comparison of recorded and simulated CdZnTe spectra. A) Recorded 60 keV spectrum from ^{241}Am . B) Simulated ^{241}Am spectrum. C) Recorded 122 keV and 136 keV ^{57}Co spectrum. D) Simulated ^{57}Co spectrum. Here $\mu_e\tau_e = 5 \times 10^{-3} \text{ cm}^2 \text{ V}^{-1}$ and $\mu_h\tau_h = 3 \times 10^{-5} \text{ cm}^2 \text{ V}^{-1}$.

electrons which are in turn the result of cosmic ray interactions (the decay of charged mesons or the decay of neutral pions followed by pair production). These gamma-rays can penetrate shielding and interact in the detector or surrounding material by photoelectric absorption, Compton scattering, and pair production. All of these processes can generate background counts in the detector, and this we refer to as “shield leakage.”

The total cosmic and atmospheric gamma-ray flux at balloon altitudes has been measured by many experiments and summarized in a paper by Gehrels.¹³ We adopt the Gehrels parameterization at 3.5 g cm^{-2} as the input spectrum to our GEANT simulations. This spectrum depends on zenith angle, slightly increasing in flux for upward-going gamma-rays since much of the production occurs in the air below the payload. The parameterization is uncertain by a factor of 1.4-2, especially above a few 100 keV.¹⁵ A parameterization is also given for a depth of 5 g cm^{-2} , but it differs from the 3.5 g cm^{-2} spectrum by only $\sim 20\%$, and then only at 10 MeV, where the uncertainties approach a factor of 2. We therefore do not expect the recorded spectrum at 5 g cm^{-2} to differ significantly from the spectrum at 3.5 g cm^{-2} , and this agrees with our observations (see Sect. 3). We restrict our modeling to the 3.5 g cm^{-2} case for simplicity, however. The gamma-ray photons are introduced on the outside of the aluminum pressure vessel and allowed to interact via the processes listed above in all the materials in the detector and surrounding structures. The total energy deposited in both the CdZnTe and the BGO for each event are finally recorded.

4.2.2. Locally Produced Gamma-Rays

The same processes that produce gamma-rays in the atmosphere also generate photons in the payload materials, namely bremsstrahlung of electrons from the atmosphere as well as secondary electrons produced in the payload mass by cosmic rays. (Electrons generated in the payload by external gamma-rays are included in the shield leakage component, described above.) Interactions in active shielding materials will generally be self-vetoed, but gamma-ray production in passive materials will contribute to the background as long as the path of the primary electron through the passive material does not also take it through an active shield. Since the electron fluxes at balloon altitudes are poorly-determined and it is difficult to calculate their production by cosmic ray interactions in the payload, we adopt the common practice of assuming that the gamma-ray production by electrons in different materials is the

same as that at a given depth in the atmosphere, with a normalization depending on the material’s atomic number. We use the gamma-ray production per unit mass of air given by Dean²² and scale it according to the material’s radiation length in g cm^{-2} .¹⁵ The photons are then produced throughout the passive materials in the detector and propagated using GEANT as before. In order to reproduce both the total and the non-vetoed spectra, a geometric correction is applied to reduce the non-vetoed counts by the fraction of solid angle at the passive material that is subtended by the BGO. The main EXITE2 phoswich detector was approximated as an 85 kg block of aluminum 1.5 m below the pressure vessel to see whether local production in the gondola structures contributed to the background.

4.2.3. Neutron-Induced Background

Another product of cosmic ray interactions in the atmosphere and in the payload is a flux of neutrons that may interact in the detector due to inelastic scattering or nuclear reactions. The background due to elastic scattering has been found to be negligible in CdZnTe due to the high atomic weight of Cd and Te.¹⁵ Neutron effects become more important in experiments using thick active shielding, since the gamma-ray contributions are effectively reduced. Since they are neutral particles, neutrons may penetrate such shielding without generating a veto. The nuclear (n,γ) reaction has a high cross section in Cd for thermal neutrons below 0.4 eV: the nucleus absorbs a neutron and is excited to ~ 8 MeV (the neutron binding energy) above the ground state. The nucleus de-excites immediately, emitting ~ 4 gamma-rays which may then Compton scatter in the CdZnTe. The thermal neutron flux from the atmosphere is small (roughly 10^{-3} neutrons $\text{cm}^{-2} \text{s}^{-1}$ at 0.5 eV,²³ which, if each produces 4 gamma-rays at 2000 keV that Compton scatter into a flat continuum below this energy, will generate only $\sim 2 \times 10^{-7}$ cts $\text{cm}^{-2} \text{s}^{-1} \text{keV}^{-1}$ in the detector), and so we do not expect the (n,γ) reaction to contribute much to the detector background. If, however, there were a local source of thermal neutrons, this reaction might become important. We discuss this, as well as a crude measurement we made on this flight of atmospheric neutron fluxes, in a forthcoming paper. Inelastic scattering excites the nucleus of the target atom through the (n,n',γ) reaction, and ~ 3 de-excitation photons are emitted with mean energies lower than those generated in the (n,γ) reaction. Both of these reactions emit “prompt” gamma-rays which may be vetoed by an active shield. Radioactive isotopes may be produced by nuclear reactions (“activation”) which result in delayed gamma-rays that cannot be vetoed by active shielding; although this component has been studied previously,¹⁵ it is complicated and not a major factor below several hundred keV, so we neglect it here.

The neutron contribution to the background is difficult to estimate accurately, and since previous attempts to model CdZnTe flight data with active shielding using neutron calculations have proved difficult,¹⁵ we do not attempt to calculate this component in detail here. Rather, we compare our gamma-ray calculations to the observed spectrum to see whether neutron effects can reasonably be responsible for the difference.

4.3. Simulation Results

The results of our GEANT simulations of the gamma-ray components of the CdZnTe/BGO detector background are shown in Fig. 4, compared to the actual measurements, between 20 and 300 keV. Fig. 4a shows the “good,” or non-vetoed spectra, and Fig. 4b shows the total spectra. A CdZnTe event was considered to be vetoed if more than 30 keV was deposited anywhere in the BGO. The contributions from shield leakage and local gamma-ray production are shown separately. The non-vetoed background (Fig. 4a) is dominated by shield leakage, and the predicted level agrees well (within a factor of 2) with the data between 30 and 300 keV. There is clearly an excess in the data below 30 keV compared to the simulation. Above ~ 100 keV the simulated spectrum seems to fall off more rapidly than the measured spectrum, but at 300 keV they are still within a factor of 2 of each other. There is a small peak in the predicted shield leakage spectrum near 70 keV, presumably due to Pb fluorescence. Though not discernible in the data, this indicates that Compton and photoelectric interactions of the primary gamma-rays in the passive material are contributing to the background. The total background predicted (Fig. 4b) is well within a factor of 2 of that measured between 30 and 100 keV, and then it too falls off more rapidly than the recorded spectrum. Shield leakage and local gamma-ray production have roughly equal magnitudes throughout the energy range shown, with local production starting to dominate at low energies. There is also evidence of a low energy excess in the data compared to the simulation. It appears that the total background has been underestimated by gamma-ray effects alone, especially above 100 keV. The simulated total spectrum is only a factor of ~ 2 greater than the simulated good spectrum at 100 keV, as opposed to a factor of ~ 6 difference in the data. We find that local production in the main EXITE2 phoswich detector does not produce a significant number of counts in the CdZnTe, since it subtends a small solid angle and is below the BGO.

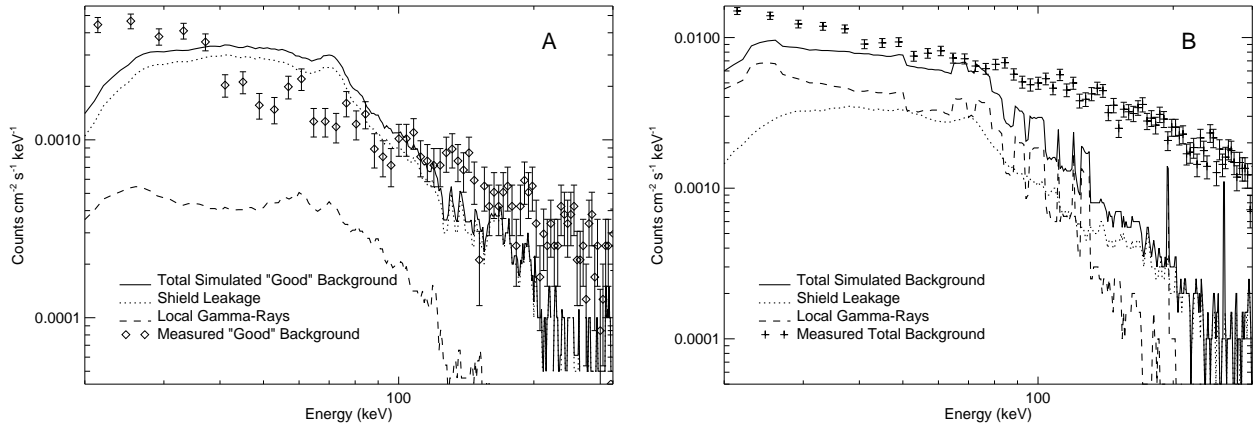


Figure 4. Comparison of the simulated spectra to the measured flight spectra for the EXITE2 CdZnTe/BGO detector. A) “Good” events (not vetoed by the BGO). B) All events. The contributions from shield leakage and local gamma-rays are indicated by the dotted and dashed lines, respectively.

5. DISCUSSION AND CONCLUSIONS

The rough agreement between the simulations and the flight CdZnTe/BGO data is encouraging: the measured and simulated good spectra lie within a factor of 2 of each other below 300 keV. Considering that the input atmospheric spectra are uncertain by factors approaching 2, especially at higher energies, this agreement is satisfactory. The results indicate that local gamma-ray production in the passive material has been effectively vetoed even by such a simple active shielding configuration. With more care, this component should be rendered completely negligible in future instruments. An active collimator, as suggested for the EXIST-LITE concept,⁷ should further reduce this source of background, as well as eliminate the contributions from fluorescence and Compton scattering.

The factor of 6 reduction in background achieved by BGO tagging is not reproduced by the simulations. This, together with the excesses at high and low energies seen in the data, and the fact that the total background is underestimated, indicates that additional components are present in the CdZnTe background that are not accounted for by gamma-ray interactions alone. These components are effectively rejected by vetoes from the BGO shield, although there is a low-energy excess seen in the good events spectrum as well. It is difficult to attribute unambiguously this good-event low-energy excess to additional background components, however, because the excess occurs near the ~ 10 keV-wide threshold of the BGO shield: low energy events that deposit little energy in the shield are less likely to be vetoed, resulting in an artificial excess in the “good” event spectrum. No such effects enter into the total spectrum, however. In Fig. 5 we show the difference between the total recorded and simulated spectra from Fig. 4b. Although this difference is highly uncertain, there is evidence of an excess below 40 keV, as well as between ~ 100 and 200 keV.

The most obvious explanation for the difference between the simulated gamma-induced spectrum and the data is provided by neutron interactions. Detailed calculations of the neutron-induced background in CdZnTe detectors in various configurations do indeed indicate that prompt neutron interactions $((n,\gamma), (n,n',\gamma))$ contribute to the background below about 50 keV¹⁵; however, this background is always at a level far lower than that indicated by Fig. 5 ($\sim 10^{-4}$ cts $\text{cm}^{-2} \text{s}^{-1} \text{keV}^{-1}$ at 20 keV, as opposed to $\sim 10^{-2}$ cts $\text{cm}^{-2} \text{s}^{-1} \text{keV}^{-1}$ in the figure). As shown in Sect. 4.2.3, the thermal component is expected to be completely negligible unless a bright source of thermal neutrons other than the atmosphere is present. Radioactive decay of the products of neutron activation can contribute to the background up to many hundreds of keV, but again at a level far below what is seen here. It is possible, however, that radioactive decay of activation products in the BGO shield itself is producing a large high energy background in the CdZnTe. This background would certainly be efficiently vetoed. It remains to be seen whether more detailed estimates of the neutron contribution to the CdZnTe/BGO detector background can provide an explanation for the large measured background and its marked reduction with the BGO shield.

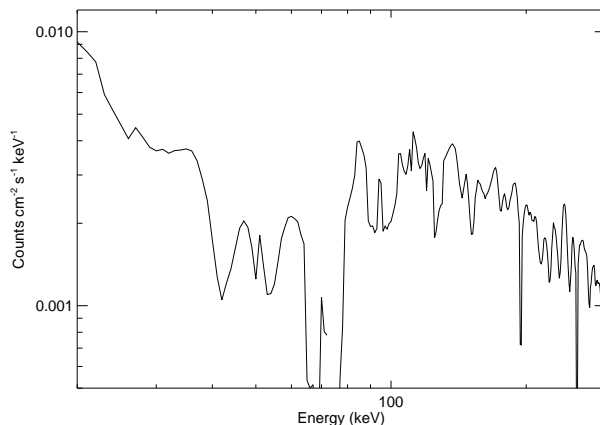


Figure 5. Residual background obtained by subtracting the total predicted background (Fig. 4b) from the total measured background. There are clearly excesses at high and low energy.

As noted in Sects. 3 and 4.2.1, we do not observe a measurable difference between the background spectra at 3.55 g cm^{-2} and $5\text{--}6 \text{ g cm}^{-2}$, nor do we expect to. The various observations spanned a period of 6.5 hours during the flight, and so we can rule out any change in the background due to activation effects over this period as well.

In Fig. 6 we compare the non-vetoed CdZnTe flight background spectra obtained by the EXITE2 CdZnTe/BGO detector, the GSFC PoRTIA thin (2 mm) detector,¹⁴ and the Caltech GRIP-2 CdZnTe detector.¹⁵ All three detectors were 2 mm thick, and all were uncollimated. The PoRTIA and GRIP-2 balloon flights were from Alice Springs, Australia; the data from these flights have been multiplied by 1.4 to account for the difference in geomagnetic latitude between Alice Springs and Ft. Sumner. The GRIP-2 detector, as noted in Sect. 2, was passively shielded by Pb-Sn-Cu with thicknesses of 5 mm, 2 mm, and 2 mm, respectively (i.e., thicker than the EXITE2 CdZnTe/BGO detector shield). The PoRTIA data shown were obtained with the CdZnTe detector sitting within the GRIS anticoincidence shield so that it was surrounded on 5 sides by 15 cm of NaI. The top of this enclosure could be covered with a 15 cm thick NaI blocking crystal (BC) or left open to provide a $75^\circ \times 100^\circ$ field of view; spectra from both modes are shown. The background levels from the three instruments are all within an order of magnitude of each other, and their relative magnitudes appear to make sense: the passively-shielded background from GRIP-2 is the highest, the partially actively-shielded EXITE2 spectrum is roughly between the other two, and the totally actively-shielded PoRTIA spectrum is the lowest. Their values at 100 keV are roughly $3.5 \times 10^{-3} \text{ cts cm}^{-2} \text{ s}^{-1} \text{ keV}^{-1}$, $9.0 \times 10^{-4} \text{ cts cm}^{-2} \text{ s}^{-1} \text{ keV}^{-1}$, and $2.8 \times 10^{-4} \text{ cts cm}^{-2} \text{ s}^{-1} \text{ keV}^{-1}$, respectively. The GRIP-2 spectrum was successfully modeled as being dominated by local gamma-rays produced in the passive material.¹⁵ The simulations presented in this paper indicate that shield leakage through the thinner lead, tin, and copper and the subsequent gamma-ray interactions in the passive material are the primary contributions to the background of the EXITE2 detector. An attempt to model the BC closed PoRTIA spectrum, including all the effects of neutron interactions, predicted a background roughly an order of magnitude lower than that observed below 100 keV.¹⁵ Indeed, the predicted CdZnTe background for this case is similar to the continuum spectrum measured by the GRIS Ge spectrometer that was flown next to PoRTIA within the NaI shield.¹⁴ It would seem, again, that CdZnTe suffers from internal background processes that are not yet understood. It is hard to see what these might be other than neutron interactions, although the neutron calculations used to model the PoRTIA background are quite detailed.

We are able to reproduce the PoRTIA BC open spectrum by adding to the BC closed spectrum the photoelectrically absorbed aperture flux from the $75^\circ \times 100^\circ$ field of view. This is shown in Fig. 6 as well. We assume that any Compton scattering events in the CdZnTe will produce a veto in the surrounding NaI. Future balloon-borne CdZnTe telescopes with active shielding and wide fields of view might use this same method to estimate their instrumental backgrounds: the PoRTIA BC closed spectrum can be taken as an estimate of the minimum achievable background level due to volume-dependent processes in the absence of passive materials, and the aperture flux due to atmospheric and diffuse cosmic gamma-rays that will be photoelectrically absorbed at each energy can be added.

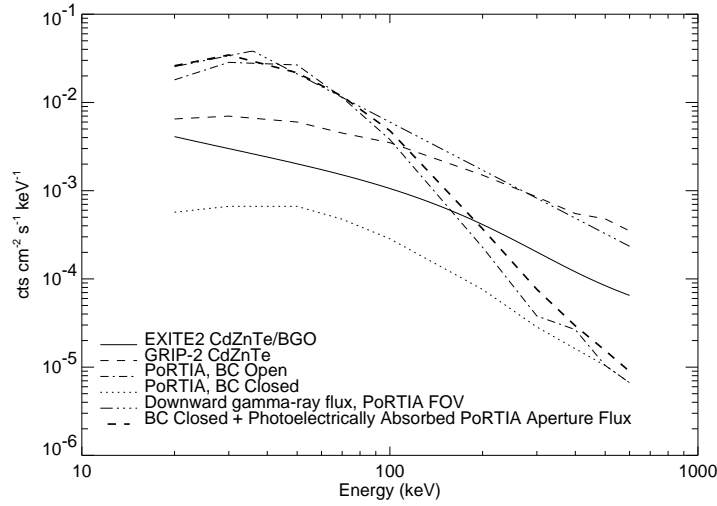


Figure 6. Comparison of CdZnTe flight spectra measured by EXITE2, PoRTIA, and GRIP-2. The PoRTIA and GRIP-2 spectra have been re-normalized to the geomagnetic latitude of Ft. Sumner. The PoRTIA spectrum is for the thin (2 mm) detector and is shown with the blocking crystal (BC) both open and closed. The BC open PoRTIA spectrum is well-reproduced by adding the aperture flux to the BC closed spectrum.

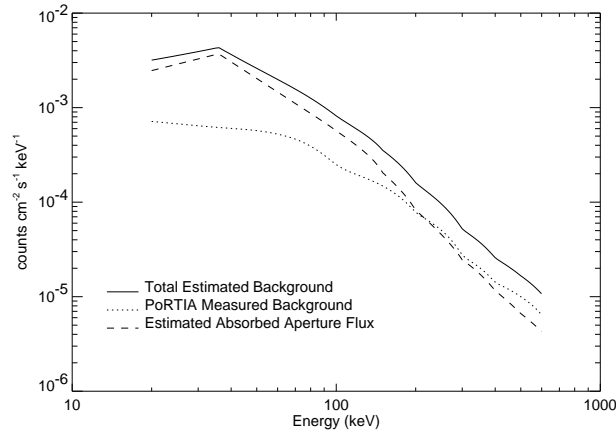


Figure 7. Estimated background for the EXIST-LITE concept, obtained by adding the expected aperture flux ($40^\circ \times 40^\circ$ field of view) that is photoelectrically absorbed in 5 mm of CdZnTe to the background measured by the thick PoRTIA detector with the blocking crystal closed. The background levels are appropriate for Alice Springs.

One such instrument is the EXIST-LITE concept,⁷ which would use 2–4 wide field ($40^\circ \times 40^\circ$ FOV, FWHM) coded aperture telescopes with 1600–2500 cm² of CdZnTe as a detector plane to perform a sensitive all-sky survey during an ultra-long duration balloon (ULDB) flight. The detector plane would be assembled from 12 mm \times 12 mm pixellated elements of CdZnTe tiled into 8 \times 8 modules, with each module sitting within a CsI collimator that doubles as an active shield. The absence of a passive collimator should reduce the background due to Compton and photoelectric interactions, as indicated by the EXITE2 CdZnTe/BGO results. The background estimate obtained by adding the aperture flux from a $40^\circ \times 40^\circ$ field of view to the PoRTIA background is shown in Fig. 7. The CdZnTe is assumed to be 5 mm thick (for response up to 600 keV), so the PoRTIA thick (5 mm) detector spectrum was used and adjusted to Alice Springs. The transmission of a tantalum coded aperture mask is included and reduces the incident

aperture flux by half at low energies. The background at 100 keV is $\sim 8.2 \times 10^{-4}$ cts $\text{cm}^{-2} \text{s}^{-1} \text{keV}^{-1}$. This level is roughly 30% greater than the background measured by the EXITE2 CdZnTe/BGO detector (the large aperture flux compensates for the lack of passive material), and is a factor of ~ 2.8 higher at 100 keV than the background recorded during the Ft. Sumner balloon flight by the EXITE2 NaI/CsI phoswich detector ($\sim 4 \times 10^{-4}$ cts $\text{cm}^{-2} \text{s}^{-1} \text{keV}^{-1}$), rescaled to Alice Springs. (The EXITE2 data and other details of the flight will be presented elsewhere.²⁴)

To make a more meaningful comparison, we consider the background appropriate to the EXITE2 field of view ($4.5^\circ \times 4.5^\circ$ FWHM). The absorbed aperture flux is only 10^{-5} cts $\text{cm}^{-2} \text{s}^{-1} \text{keV}^{-1}$ at 100 keV in this case, and so the instruments are not aperture dominated and the PoRTIA background may be compared directly to the EXITE2 phoswich background. This gives a CdZnTe background of $\sim 3.6 \times 10^{-4}$ cts $\text{cm}^{-2} \text{s}^{-1} \text{keV}^{-1}$ at 100 keV, roughly equal to that of the phoswich. (These rough estimates obviously do not consider differences in shield leakage between the two experiments.) Thus, with proper shielding, CdZnTe is a reasonably low-background material, with levels comparable to current scintillators. We expect that ULDB balloon flights or space missions employing CdZnTe detectors should be able to achieve high-sensitivity astronomical observations in the hard X-ray range with good spatial and spectral resolution. If the high CdZnTe backgrounds observed without active shielding are indeed due to neutron interactions, one additional method of reducing this background even further may be the use of “supershields,”²⁵ which use layers of low-Z material to moderate neutrons before they are stopped by a layer of an efficient neutron-absorber.

We have made a measurement of the background recorded by a CdZnTe detector flown at balloon altitudes in a configuration approximating a plausible hard X-ray instrument. The active BGO shield behind the detector enables a large reduction in the CdZnTe background to a level comparable to that of current phoswich detectors. Shield leakage and gamma-ray interactions in the passive material in front of the detector make up a significant portion of the recorded good spectrum, but there are clearly additional components to the total CdZnTe/BGO detector background that are effectively vetoed. It is not clear that neutron interactions as currently understood can account for the difference; it is possible that activation in the BGO contributes at high energies. Future hard X-ray missions employing CdZnTe detectors may benefit from active collimators and supershields. Further effort to understand the background in CdZnTe detectors is needed, as the good spectral and spatial resolution possible with this material make it very valuable to the future of hard X-ray astronomy. We will continue our own efforts by flying a small pixellated CdZnTe detector array surrounded by a CsI shield on the next EXITE2 balloon flight in 1999 in preparation for construction of a large-area CdZnTe array (EXITE3) for use in a balloon-borne coded aperture telescope.

ACKNOWLEDGMENTS

We thank B. Matthews for work on the CdZnTe detector, T. Gauron and J. Grenzke for work on the flight electronics and software, and K. Lum for work on the data analysis software. This work was supported in part by NASA grant NAG5-5103. P. Bloser acknowledges support from NASA GSRP grant NGT5-50020.

REFERENCES

1. J. Butler, C. Lingren, and F. Doty, “CdZnTe gamma ray detectors,” *IEEE Trans. Nucl. Sci.* **39**, p. 605, 1992.
2. H. Barrett, J. Eskin, and H. Barber, “Charge transport in arrays of semiconductor gamma-ray detectors,” *Phys. Rev. Lett.* **75**, p. 156, 1995.
3. A. Parsons, C. Stahle, C. Lisse, S. Babu, N. Gehrels, B. Teegarden, and P. Shu, “Room temperature semiconductor detectors for hard x-ray astrophysics,” *Proc. SPIE* **2305**, p. 121, 1994.
4. C. Stahle, Z. Shi, K. Hu, S. Barthelmy, S. Snodgrass, L. Bartlett, P. Shu, S. Lehtonen, and K. Mach, “Fabrication of CdZnTe strip detectors for large area arrays,” in *Hard X-ray and Gamma-Ray Detector Physics, Optics, and Applications*, B. Hoover and F. Doty, eds., *Proc. SPIE* **3115**, p. 90, 1997.
5. J. Matteson, W. Coburn, F. Duttweiler, W. Heindl, G. Huszar, P. Leblanc, M. Pelling, L. Peterson, R. Rothschild, R. Skelton, P. Hink, and C. Crabtree, “CdZnTe arrays for astrophysics applications,” in *Hard X-ray and Gamma-Ray Detector Physics, Optics, and Applications*, B. Hoover and F. Doty, eds., *Proc. SPIE* **3115**, p. 160, 1997.
6. J. Grindlay, T. Prince, N. Gehrels, J. Tueller, C. Hailey, B. Ramsey, M. Weisskopf, P. Ubertini, and G. Skinner, “Energetic X-ray Imaging Survey Telescope (EXIST),” *Proc. SPIE* **2518**, p. 202, 1995.
7. J. Grindlay, “Balloon-borne hard x-ray imaging and future surveys,” *Adv. Space Res.* **21**, p. 999, 1998.

8. P. Bloser, T. Narita, J. Grindlay, and K. Shah, "Prototype imaging Cd-Zn-Te array detector," in *Semiconductors for Room-Temperature Radiation Detector Applications II*, R. James, T. Schlesinger, P. Siffert, M. Cuzin, M. Squillante, and W. Dusi, eds., *Proc. MRS* **487**, p. 153, 1998.
9. T. Narita, P. Bloser, J. Grindlay, R. Sudharsanan, C. Reiche, and C. Stenstrom, "Development of prototype pixellated PIN CdZnTe detectors," in *Hard x-ray and gamma-ray detector physics and applications*, *Proc. SPIE* **3446**, p. 218, 1998.
10. P. Charalambous, A. Dean, R. Lewis, and N. Dipper, "The background noise in space borne low energy gamma-ray telescopes," *Nuc. Inst. Meth. A* **238**, p. 533, 1985.
11. J. Matteson, P. Nolan, W. Paciesas, and R. Pelling, "Design and performance of an actively collimated phoswich system for x-ray astronomy," *Space Sci. Instr.* **3**, p. 491, 1977.
12. A. Dean, F. Lei, and P. Knight, "Background in space-borne low-energy gamma-ray telescopes," *Space Sci. Rev.* **57**, p. 109, 1991.
13. N. Gehrels, "Instrumental background in balloon-borne gamma-ray spectrometers and techniques for its reduction," *Nuc. Inst. Meth. A* **239**, p. 324, 1985.
14. A. Parsons, S. Barthelmy, L. Bartlett, F. Birsa, N. Gehrels, J. Naya, J. Odom, S. Singh, C. Stahle, J. Tueller, and B. Teegarden, "CdZnTe background measurements at balloon altitudes," *Proc. SPIE* **2806**, p. 432, 1996.
15. F. Harrison, C. Hailey, J. Hong, A. Wong, and W. Cook, "Background in balloon-borne hard x-ray/soft gamma-ray cadmium zinc telluride detectors," *Nuc. Inst. Meth. A*, in press.
16. K. Slavis, W. Binns, P. Dowkontt, J. Epstein, P. Hink, J. Matteson, F. Duttweiler, G. Huszar, P. Leblanc, M. Pelling, R. Skelton, and E. Stephan, "High altitude balloon flight of CZT detectors for high energy x-ray astronomy," *BAPS* **43**, p. 1087, 1998.
17. K. Lum, R. Manandhar, S. Eikenberry, M. Krockenberger, and J. Grindlay, "Initial performance of the EXITE2 imaging phoswich detector/telescope for hard x-ray astronomy," *IEEE Trans. Nucl. Sci.* **NS-41**, p. 1354, 1994.
18. K. Hecht, "Zum Mechanismus des Lichtelektrischen Primarstromes in Isolierenden Kristallen," *Zeits. Phys* **77**, pp. 235-243, 1932.
19. Z. He, G. Knoll, and D. Wehe, "Direct measurement of electron drift parameters of wide band gap semiconductors," *Nuc. Inst. Meth. A*, in press.
20. P. Luke, "Unipolar charge sensing with coplanar electrodes - applications to semiconductor detectors," *IEEE Trans. Nucl. Sci.* **42**, p. 207, 1995.
21. O. Tousignant, L. Hamel, J. Courville, P. Paki, J. Macri, K. Larson, M. Mayer, M. McConnell, and J. Ryan, "Progress in the study of CdZnTe strip detectors," in *Hard X-ray and Gamma-Ray Detector Physics, Optics, and Applications*, B. Hoover and F. Doty, eds., *Proc. SPIE* **3115**, p. 214, 1997.
22. A. Dean, F. Lei, K. Byard, A. Goldwurm, C. Hall, and J. Harding, "The gamma-ray emissivity of the Earth's atmosphere," *Astron. Astrophys.* **219**, p. 358, 1989.
23. T. Armstrong, K. Chandler, and J. Barish, "Calculations of neutron flux spectra induced in the Earth's atmosphere by galactic cosmic rays," *J. Geophys. Res.* **78**, p. 2715, 1973.
24. Y. Chou, P. Bloser, J. Grenzke, J. Grindlay, K. Lum, G. Monnelly, and B. Robbason, "EXITE2 detector and telescope development and initial balloon flight results," *IEEE Trans. Nucl. Sci.*, in preparation.
25. C. Hailey and F. Harrison, "A new concept for background rejection in gamma-ray astronomy - the supershield," *Nuc. Inst. Meth. A* **365**, p. 518, 1995.